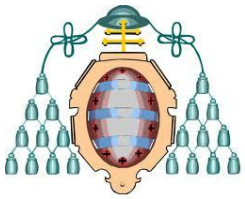

UNIVERSIDAD DE OVIEDO

MASTER IN CONDENSED MATTER PHYSICS & NANOTECHNOLOGY

Construction and characterization of a temperature-controlled fluid cell for single-molecule studies with Magnetic Tweezers

Master's Thesis

realized at
Centro Nacional de Biotecnología (CNB-CSIC, Madrid)

Submitted by:
Francesca Zuttion

Academic Year: 2011/2012
Submission date: 25th June 2012

Internal Supervisor: Dr. María Vélez Fraga (Univ. Oviedo)
External Supervisor: Dr. Fernando Moreno Herrero (CNB-CSIC)
Tutor: M.Sc. Benjamin Gollnick (CNB-CSIC)

Abstract

An important class of enzymes that is object of single-molecule biophysics studies is the one formed by proteins called helicases. Helicases are molecular motors that move along double-stranded DNA unwinding the two strands using the energy of ATP. These motor proteins can have different structural compositions that influence their function, but all of them have the property that their activity depends on the temperature of the surrounding medium. Our goal is to study how the activity of the helicase-nuclease complex AddAB is influenced by temperature, using a Magnetic Tweezers (MT) setup. With the aim of controlling the temperature inside the sample cell with a precision of 0.1 °C, a modified version of the current MT sample cell has been constructed and characterized. Briefly, the sample cell consists of two glass cover slides sealed by two layers of Parafilm. This assembly is coupled to liquid inlets and outlets by a metal baseplate and a plastic sample holder. The channel created between the two glass layers is accessed through two holes made in the upper cover glass and enables flushing buffer inside the fluid cell to study the activity of biological samples. In order to control the temperature of the system two thin-foil resistive heaters have been attached to the bottom part of the baseplate, and using a high-precision sensor the temperature of the baseplate has been monitored. The setup is controlled by customized LabVIEW software that contains a PID feedback, through which the voltage applied to the heaters is regulated and the heating process is monitored. The results presented in this thesis correspond to calibration measurements and finite-element simulations. We have found that both *in-silico* and experimental measurements are in good agreement.

Contents

1. Introduction

The fundamental request of understanding the molecular basis of life makes it necessary to comprehend the structure and function of complex biological macromolecules like proteins. At the state of the art, scientists have a lot of tools to investigate, for example, the processes associated with molecular motors that are able to convert chemical energy into mechanical work. The desire to monitor the behavior of individual biomolecules in real time has given rise to the development of more and more precise single-molecule manipulation techniques, now capable of measuring forces in the (sub-) piconewton range [1]. The most commonly used are Optical Tweezers, Atomic Force Microscopy and Magnetic Tweezers [1]: they are complementary techniques, in terms of the force range and spatial resolution; therefore, depending on the application, one is able to choose the best suited one.

1.1 Magnetic Tweezers

Magnetic Tweezers (MT) is a technique that allows probing the mechanical properties of nucleic acids and protein-nucleic interactions in real time at the single-molecule level [2] [3]. Briefly, a MT setup mounted on a customized inverted optical microscope is able to detect the positions of micrometer-sized magnetic spheres (commonly called “beads”) in three-dimensions with a precision of a few nanometers while applying forces from a few tenths to tens of piconewtons [4].

To achieve this, in our setup two permanent magnets are used to generate a magnetic field gradient able to exert a force on the beads. The microspheres are connected with the glass surface of the fluid cell through a DNA filament that is functionalized with biotin at one end (to form a bond with a streptavidin-coated bead) and with digoxigenins at the other end (to fix this end to an anti-digoxigenin coated surface). By moving the magnets along and rotating them around the vertical (optical) axis, it is possible to change the force applied on the beads and to induce torque in the DNA molecule, respectively. Both effects are detected via the variation of the end-to-end distance between the tethered microsphere and a reference sphere glued to the bottom glass surface (see Fig. 1.1).

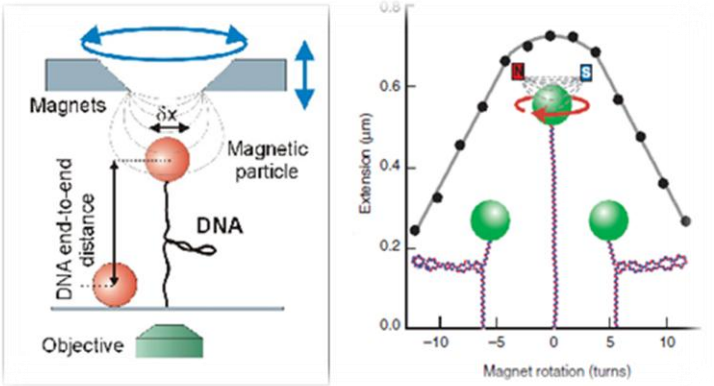

Fig. 1.1: *Schematic pictures of how a MT operates, taken from www.biotec.tu-dresden.de and Ref. [1].*

The bead is subjected to a force $\vec{F}$ that is given by the negative gradient of the potential energy *U*, which in the presence of an external magnetic field $\vec{B}$, induces a magnetic moment $\overrightarrow{m_b}$ in the bead.

$$U = -\frac{1}{2}\,(\overrightarrow{m_b} \cdot \vec{B}) \tag{1}$$

$$\vec{F} = -\vec{\nabla}U = \frac{1}{2}\,\vec{\nabla}(\overrightarrow{m_b} \cdot \vec{B}) \tag{2}$$

Since the field of view of the optical image is small compared to the distance between both magnets, we can assume that magnetic field lines are equally spaced near the bead. Therefore, experiments are done at constant force [2].

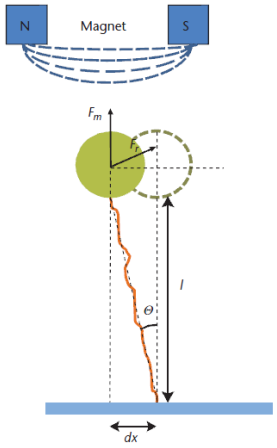

Fig. 1.2: *Schematic picture of the bead-DNA system subjected to a magnetic pulling force F_m in the vertical direction, taken from Ref. [2].*

To determine the force applied to the bead, its Brownian motion must be analyzed. The bead is pushed out from its equilibrium position due to random collisions with the surroundings water molecules, with displacement amplitudes that strongly depend on the applied force. As shown in Fig. 1.2, if the displacement d*x* is small with the respect to the height above the surface *l*, the restoring force F_r is also small and can therefore be approximated by $F_m\theta$, where F_m is given by the magnetic field. If we furthermore approximate θ by $\frac{dx}{l}$, then the restoring force can be written as $F_r = F_m\frac{dx}{l}$. The system can be thought of as an elastic spring with spring constant $k = \frac{F_m}{l}$ and elastic energy $E = \frac{1}{2}k\langle dx^2\rangle$, where $\langle dx^2\rangle$ is the mean square displacement of the Brownian motion. According to the equipartition theorem, $= \frac{1}{2}k_B\,T$, we obtain that

$$F_m = \frac{k_B\,lT}{\langle dx^2\rangle}\,. \tag{3}$$

Microsphere positions are determined by video-tracking. The *xy* position of a bead is determined from the center of mass of the optical image. The position along the *z*-axis is determined from the diffraction rings of the tethered bead. A 360° averaged radial intensity profile from the center of the bead can be calculated and compared with that of a reference bead lying on the glass surface [2]. Direct comparison of both profiles leads to a distance along the z-axis.

MT presents some advantages with respect to other force spectroscopy techniques. For example, it does not suffer from sample heating and photodamage due to the fact that no laser sources are used. Also, it is possible to work with several particles at the same time, and the presence of the permanent magnets allows the combination of force clamp properties with the ability to impose rotation [1]. All these properties make MT a good tool to study mechanical properties of DNA and DNA-protein interactions.

1.2 Single-molecule studies of the molecular motor AddAB

Helicases form an important class of enzymes for all living organism. The first one was discovered in 1976 in *E. coli* bacteria, and since then they have been found in all forms of life [5]. Briefly, they use the energy from ATP hydrolysis to stably separate the strands of nucleic acids, to remove nucleic acid-associated proteins, and to catalyze homologous DNA recombination [5]. There is a great interest in understanding the mechanisms behind their activity, not only due to their importance in cellular processes but also because they represent a prototype of ATP-coupled molecular motors.
A model helicase is the *B. subtilis* AddAB helicase-nuclease which prepares double-stranded DNA breaks for repair by homologous recombination. To do this, the presence of a particular DNA sequence (referred to as "Chi", an abbreviation for crossover hotspot instigator) is needed to attenuate the activity of one of the nuclease domains of the AddAB complex which leads to the formation of a single-stranded DNA overhang [5]. AddAB is composed of two protein subunits: AddA and AddB. AddA contains one nuclease domain and motifs of Superfamily I helicases, while the AddB subunit contains a nuclease domain only (see Fig. 1.3).

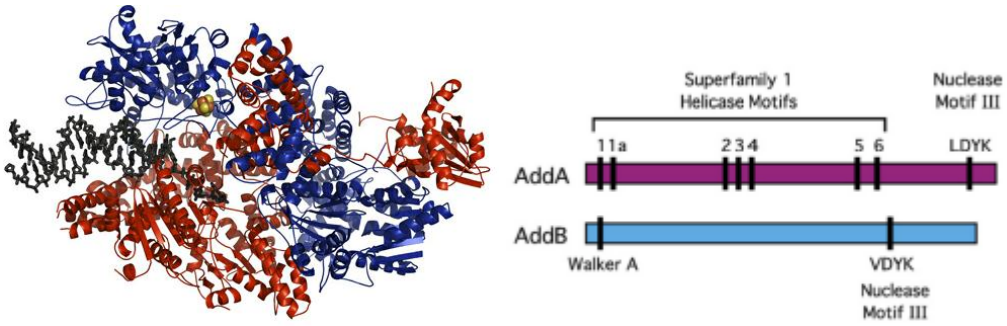

Fig 1.3: *3D model and schematic representation of the subunits of the AddAB complex, taken from Ref. [7] and Ref. [8], respectively.*

The activity of this enzyme is still object of investigation. In a recent study it was shown that since AddAB contains only one complete set of helicase motifs (in the AddA subunit) it functions as a helicase with a single motor only [9].
One of the research lines of the group in which this M.Sc. thesis has been elaborated is related to the activity of the AddAB complex. Recently, in a work still in progress, the translocation of the AddAB has been monitored using MT. However, it was found that temperature plays an important role in the translocation properties of the enzyme. Since the ambient temperature in our laboratory may vary from one day to another, a wide dispersion of the translocation velocity is observed. Therefore, comparison of data from different days becomes difficult. This has motivated the development of a device to control the temperature at which the experiment is done.
The MT technique has been used to investigate other DNA-translocating motors. For instance, in 2008, R. Seidel et al. [10] applied MT to study the translocation rate of Type I restriction enzyme *Eco*R124I, which also moves along double-stranded DNA but with a completely different mechanism. They also studied the system as a function of the environmental conditions: they changed the temperature to understand how

this affects the process of translocation. They found that i) the duration of the motor event decreases with increasing temperature, ii) the enzyme speed changes with the temperature, and iii) the step size is temperature-independent. In their experiments, temperature control was achieved by regulating the ambient temperature of the room, the temperature of the microscope objective via an objective heater and the temperature of the fluid cell via transparent heating elements located on top of the cell.
In a similar but potentially more efficient way, we want to control the temperature of the system in order to find a relation between this physical quantity and the characteristic parameters of the motion of the AddAB protein along the DNA. Furthermore, the control of the temperature can help us to improve the translocation signal by decreasing the signal dispersion during measurements. We will also explore if changes in temperature can affect our force measurements, as might be expected from Eq. 3.

1.2 Goal and Outline

The goal of this project is to build a sample cell for our MT to control the temperature during DNA-protein experiments with a precision of 0.1 °C. The outline of this thesis is as follows. In chapter 2, the experimental setup is described. In chapter 3 the results obtained from simulations based on finite-element analysis and calibration experiments are presented. The experimental data discussed here represent preliminary tests of the system, necessary to reach the final goal of this project. In the last chapter, the results are discussed and the future steps illustrated.

2. Materials and Methods

In order to heat up the fluid cell, two resistive foil heaters (MINCO polyimide heaters HK5160R5.6L12E) are glued to the bottom part of a stainless steel baseplate. These resistances are connected in series to a programmable power supply (TTi PL303-P). The temperature is measured with two temperature sensors (Correge Pt100 sensors PTFC101T), which are positioned at two different points of the baseplate: one near the sample cell and one close to the heating foils. Each of them is connected to a temperature converter (Brodersen signal converter PXT-10.924), whose voltage signal is read using a data acquisition (DAQ) device (National Instruments cDAQ-9171 chassis with 9215 analog input module). Both the power supply and the DAQ module are controlled with a PC using a custom-made LabVIEW program that contains a PID feedback.

2.1 Fluid cell

The fluid cell used in our MT is shown in Fig. 2.1. It is made of two cover slips separated by two layers of Parafilm (thickness∼200 µm). A channel is created by leaving a volume of ∼100 µl between the Parafilm and the glass surfaces. The upper cover slip presents two inlets, in order to allow the exchange of fluids. A laser cutter is used to create the inlet holes in the cover glass and the channel geometry in the Parafilm layer.

To assemble all the parts, two cover slips (one of them with inlet holes and one without) are cleaned via sonication for 10 min in isopropanol and then dried with air. Two previously cut layers of Parafilm are placed between the cover glasses, taking care that all the edges are well aligned. The assembly is placed onto a heating plate at 150 °C for 2 min in order to melt the Parafilm, which establishes a good sealing between the glass surfaces after it has cooled down again.

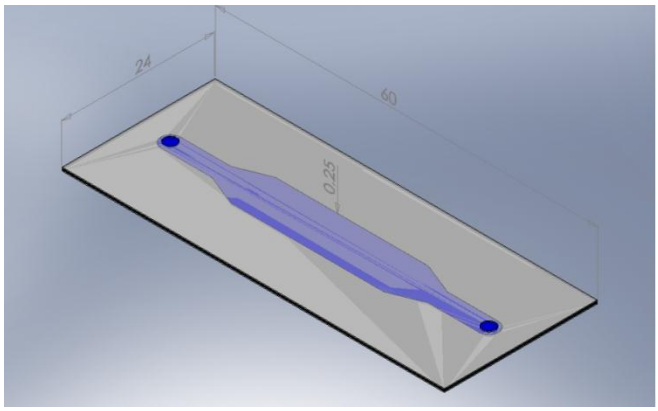

Fig. 2.1: *Technical drawing of the fluid cell, in blue is depicted the channel filled with the buffer solution (all dimensions are in mm).*

To perform experiments, the fluid cell is stably mounted between a metal baseplate and a holder part made of PEEK (Polyether Ether Ketone). Two O-rings provide a stable seal between the plastic holder and the inlets of the upper cover glass. The geometry of the top part satisfies the condition that the approach of

the magnets to the sample cell is not obstructed. The final configuration (without the adapter screws containing the O-rings and without the fluid cell) is depicted in Fig. 2.2.

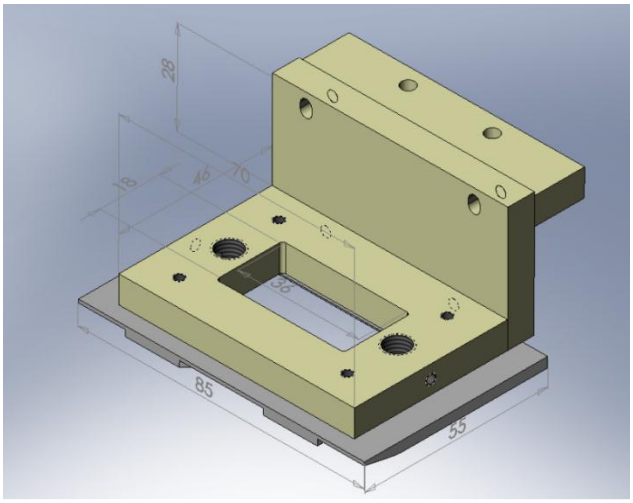

Fig.2.2: *Technical drawings of the sample cell holder assembly (all dimensions are in mm).*

2.2 Heating foils and temperature sensors

Heating foils

Heating foils are thin, flexible components consisting of an etched-foil resistive heating element laminated between layers of flexible insulation. Etched-foil heating technology provides fast and efficient thermal transfer, and the thin construction assures close thermal coupling between the heater element and the heat sink [11].

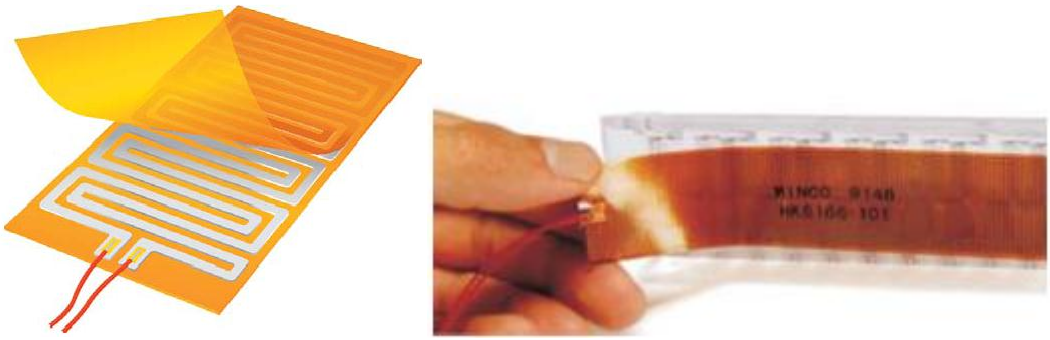

Fig. 2.3: *Schematic (left) and photograph of thermofoils, taken from Ref. [11].*

For our setup, we use polyimide heaters provided by MINCO [11]. They are rectangular (12.7 x 50.8 x 0.4 mm), have a resistance R = 5.6 Ohm and contain an aluminum layer, which makes contact with the heat sink facilitating uniform heating. Furthermore, they come with a pressure-sensitive acrylic adhesive backing that is used to stick them to the metal baseplate. These particular foils can be used within a temperature range of -32 °C to 150 °C.

The heating foils are mounted on the lower surface of the baseplate, one at each side as shown in Fig. 2.4. Special care needs to be taken during the installation because bad positioning of the heaters can have an influence on the performance of the system. It is important to create a good contact between the foils and the surface of the heat sink, in order to avoid the presence of gaps that can block the heat transfer and the formation of hot spots that can cause heating failure. We use a small quantity of thermally conductive epoxy glue to additionally fix the heater ends and leads at the edge of the baseplate, thus making the system more robust for everyday use. For fast curing of both acrylic adhesive and epoxy we heated up the system in an oven for 1 hour at 100 °C (acrylic glue) and 2 hours at 65 °C (epoxy).

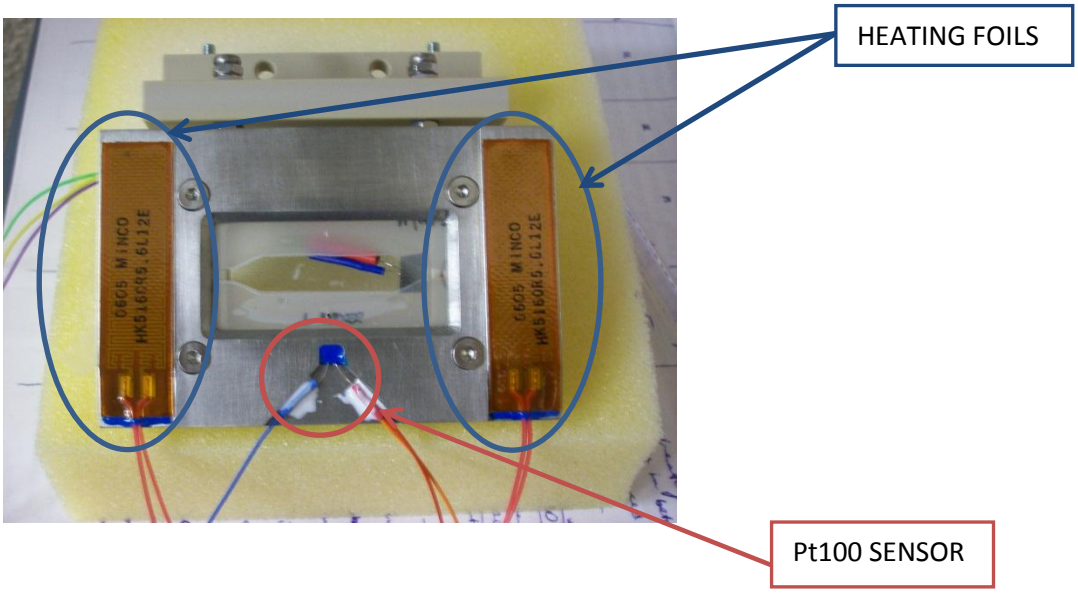

Fig.2.4: *MT base plate with heating foils and Pt100 sensor attached (see next subsection), placed on the bottom side.*

Temperature sensor

To monitor the temperature changes induced by the voltage applied to the heating foils, we use a Pt100 sensor connected to a temperature converter. Pt100 sensors are temperature transducers based on the resistance change of platinum with temperature, showing a well-defined value of 100 Ohm at 0 °C.

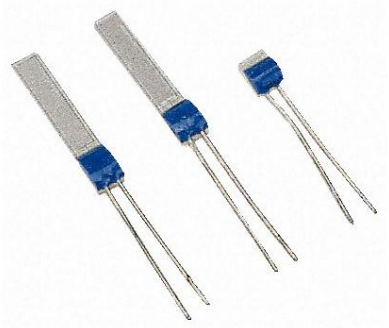

Fig. 2.5: *Image of three Pt100 sensors, taken from www.es.rs-online.com: the smaller one is the one is used in our system. Sensor specifications are: 2.0 x 2.3 mm, thickness < 1.5 mm, lead length 10 mm, readout error ±0.04 Ohm or ±0.01 °C.*

These types of sensors can work from -50 °C to 600 °C. However, for the sensor used to perform the experiments described in this thesis we restrict the temperature range to $T \in$ [-50; 100] °C, which corresponds to a linearly dependent voltage output U from the signal converter between 0 and 10 V. The two quantities are therefore related by the following equation:

$$U = \frac{50+T}{15} \tag{4}$$

Basically, the resistance measured by the sensor is converted into a voltage reflecting linear temperature readout. The relation between the temperature and the resistance can be approximated by:

$$R(T) = R\,(0)(1 + \alpha T), \tag{5}$$

where *R(T)* is the resistance at a given temperature *T*, *R(0)* is the resistance at 0 °C, and α is the temperature coefficient of the resistance given in $°C^{-1}$, which can be obtained knowing the values of the resistance at 0 °C and at 100 °C:

$$\alpha = \frac{R(100)-R(0)}{100°C * R(0)}. \tag{6}$$

For Pt100 sensors, H. L. Callendar first found that the linear relationship described by Eq. 5 has to be corrected by a quadratic term for $T > 0$ °C:

$$R(T) = R(0)(1 + A * T + B * T^2)\ , \tag{7}$$

where *A* and *B* are constants [9]. If negative temperatures are considered, it is necessary to add two more terms resulting in a polynomial of degree four, later described by M. S. van Dusen [12], which however is irrelevant for our experiments:

$$R(T) = R(0)(1 + A * T + B * T^2 + C(T - 100) * T^3)\ . \tag{8}$$

Both forms of the equation are commonly denoted “Calendar-van Dusen equation”. Since the relevant temperature range for us is $T \in$ [18°; 50] °C, we apply Eq. 5 and Eq. 7 to obtain a corrected temperature T_c from the recorded ones T_{nc} in our LabVIEW program (section 2.3). The acquired values T_{nc} are obtained from Eq. 4, since the physical quantity that we measure is the voltage from the Pt100 sensor:

$$T_{nc} = 15U - 50, \tag{9}$$

These values are used to calculate the resistance $R(T_{nc})$ by Eq. 5. Since this resistance has to be equal to the one that can be obtained from Eq. 7, $R(T_c)$, it is possible to establish a relation between the acquired temperature T_{nc} and the corrected one T_c:

$$T_c = \frac{-A+\sqrt{A^2+4\alpha B T_{nc}}}{2B}, \tag{10}$$

where $A = 3.9083 * 10^{-3}$ °C^{-1}, $B = -5.775 * 10^{-7}$ °C^{-2}, $\alpha = 3.85055 * 10^{-3}$ °C^{-1} [13]. These three values are the ones calculated for a sensor of 100 Ohm. Temperature coefficient α together with an additional coefficient δ is needed to derive *A* and *B*. The parameter δ was introduced by H. L. Callendar to rewrite Eq. 5 with a better approximation [14]:

$$\delta = \frac{T_h - T}{\left(\frac{T_h}{100\,°C} - 1\right) * \left(\frac{T_h}{100\,°C}\right)}, \tag{11}$$

where T_h is the actual temperature, and T is the temperature obtained from Eq. 5. Coefficients A and B will then be given by:

$$A = \alpha + \frac{\alpha * \delta}{100\ °C} \tag{12}$$

$$B = -\frac{\alpha * \delta}{(100\ °C)^2}\,. \tag{13}$$

Pt100 sensors have two main advantages: high accuracy and long-term stability, but their low resistance means that lead resistance can introduce noticeable errors. The two kinds of errors that can be observed are offset errors and changes in lead resistance with temperature. Fortunately, both of them can be overcome by the use of 3-wire or 4-wire compensation circuits [15]. The configuration that we use is the one with 3 wires, in which one wire is attached to one terminal and two wires to the other one, as depicted in Fig. 2.6. In this way, and as long as all the three cables have the same length, their resistances are the same (R_1 = R_2 = R_3). As a consequence, we can eliminate the contribution of the wires by subtracting the resistance measured between 2 and 3 (R_{23}) with the one between 1 and 2 (R_{12}), such that the measured resistance is equal to the one of the sensor R_{Pt}:

$$R_{12} = R_1 + R_{Pt} + R_2; \qquad R_{23} = R_2 + R_3 \tag{14}$$

$$R(T) = R_{12} - R_{23} = R_{Pt} + R_1 + R_2 - (R_2 + R_3) = R_{Pt} \tag{15}$$

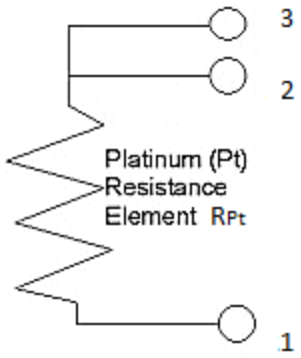

Fig. 2.6: *Schematic drawing of the 3-wire configuration, taken from www.cip.ukcentre.com. The measured resistance R(T) is given by Eq. 15.*

2.3 Computer Control and PID feedback

The power supply, the signal from the temperature converter, and the response of the system to a change are controlled via a custom LabVIEW software program containing a PID feedback.

Computer control

LabVIEW is a system design platform and development environment of a visual programming language developed by National Instruments [16]. The program developed to control the setup essentially consists in

a while loop containing three sequential frames. In the first frame the temperature readout and the PID feedback are implemented, the second frame controls the power supply, and the third one gives the system the necessary time to respond through a delay.

As depicted in Fig. 2.7, in the first frame the signal from the temperature converter is used to determine an approximate temperature value, which is then corrected using an expression (Eq. 10) derived from the Callendar-Van Dusen equation (see section 2.1). The corrected temperature and an average temperature (calculated with a variable number of elements) are monitored as functions of time. All these parameter are used for the PID feedback that will be described in the next subsection. When the temperature setpoint is changed, the very first voltage setpoint is extracted from the inverse of a previously obtained calibration curve *T* vs. *U.* With the PID controller active, in all the following iterations *i* a voltage correction is added to the setpoint of iteration *i*-1*,* and the new setpoint is passed to the second frame provided it falls within the range of allowable values. The second frame is used to set the new voltage value of the power supply and read back the real voltage and current on request. In the last frame a time delay of 0.5 s is fixed in order to define a constant sample rate of 2 Hz.

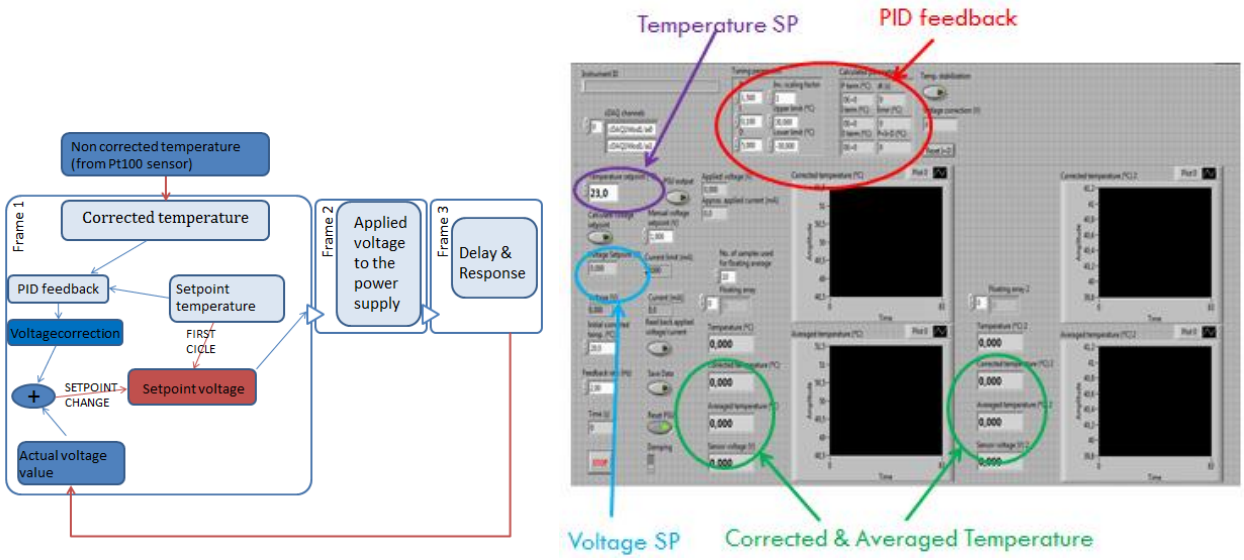

Fig. 2.7: Flowchart corresponding to the algorithm (left) *and outline of the front panel (right) of the LabVIEW software that we use.*

PID feedback

The essential subroutine that is implemented in the first frame of the while loop is the PID feedback. It is a control loop mechanism that contains a proportional (*P*), an integral (*I*) and a derivative (*D*) gain. It corrects for the differences between the measured process variable *V(t)* at time *t* and the setpoint *SP*.

There are three tuning parameters that are considered in this kind of feedback: *P*, T_I and T_D. With a correct selection of them the controller can eliminate the error *e(t) := V(t) - SP* quickly, thus preventing oscillations of the process variable. T_I is the integral time, which is related to the integral gain by $I = \frac{P}{T_I}$, and T_D is the derivative time related to the derivative gain by $D = P * T_D$. These three contributions sum up, and the equation that gives the controller output value *O(t)* is the following:

$$O(t) = P\left[e(t) + \frac{1}{T_I}(\int e(t)dt) + T_D\left(\frac{d}{dt}e(t)\right)\right], \quad (16)$$

where the first term is the proportional, the second the integral and the third the derivative one. The proportional term describes how the system reacts to the presence of the error *e(t),* the integral term accounts for the sum of all previous errors, and the derivative term corrects for the rate of change of the error. Figuring out the three tuning parameters is not easy because the best choice for one of them depends on the others and on the behavior of the controlled process. To solve this problem, J. G. Ziegler and N. B. Nichols from Taylor Instruments elaborated two procedures to empirically determine the values of the tuning parameters: the open-loop and the closed-loop method [17]. Briefly, in the closed-loop method the *P* gain at which the process starts to oscillate defines the remaining parameters, in the open-loop method the PID controller is switched off and the results of a small step change are monitored. More detailed information about these two methods will be given in the results section (chapter 3).

3. Results

In this Chapter the latest results are presented. These include i) simulations based on finite-element analysis and ii) test experiments for calibration of our system and implementation of the PID feedback (see section 2.3). An outlook on future work necessary to achieve the final goal of this project will be provided in chapter 4.

3.1 Finite-element computer simulations

To better understand how the heating process works and to obtain more information about the physics involved, we decided to perform stationary and time-dependent simulations with COMSOL Multiphysics, a finite element analysis, equation solver and simulation software for various physics and engineering applications [18]. It allows one to couple different physics phenomena, for example electric current and heat transfer, and to study how a system behaves in a visual way. Important steps while designing a model with COMSOL are the definition of the material properties and the creation of a mesh. The former determines the ground structure of a model because all physical quantities are related to the properties of the materials of the structure under study. The latter refers to the division of the system into small subunits in order to solve the differential equations related to a specific problem. We make use of the default option of *physics controlled meshing*, in order to adapt the mesh to the meshing requirement from the interfaces used in the model. In Fig. 3.1 you can see a 3D model representing the system that we use in the simulation: the baseplate material is stainless steel (see chapter 2), while the heating foils consist of two different layers each, one made of aluminum making contact with the baseplate and a second one made of insulating polyimide, which contains the resistive circuit. For this reason, in a first approximation, in our simulations we define an aluminum part with thickness 0.1 mm and a polyimide parts with thickness 0.3 mm. Fig. 3.1 also shows the position where the Pt100 sensor is attached (blue part). We have not modeled its presence, but only probe the temperature at its position.

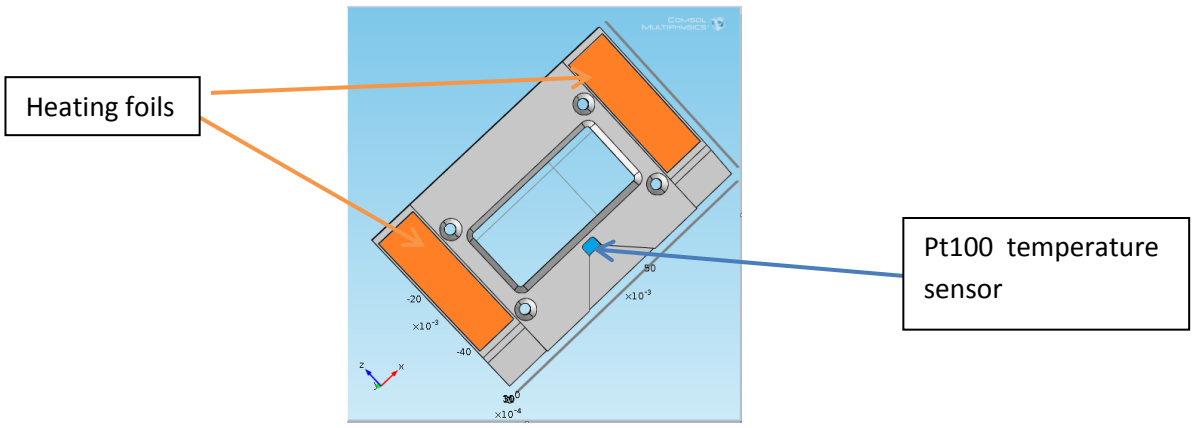

Fig. 3.1: *Drawing of the geometry implemented in the simulations.*

To simulate our system we use two modules within COMSOL: the *Electric Current Interface* (*ec*) and the *Heat Transfer in Solids Interface* (*hts*). The *ec* module is used to describe the application of a potential to

the heaters. With this interface it is possible to define the equations, the boundary conditions and the current sources to model the steady electric currents in conductive media, setting the applied electric potential as the setpoint [18]. With the *hts* interface it is possible to implement the equations, the boundary conditions and the heat sources to describe convective and conductive heat transfer, setting the temperature as the setpoint [18]. We use it to model the heat transfer from the heaters to the rest of the system and to describe the heat dissipation to the ambient air. In particular, we have used the *Heat Source* domain condition to add the contribution of the heat power generated from the *ec* interface and the *Heat Flux* condition to add the flux across the boundaries. We describe the heat dissipation to the environment with the following equation:

$$q = h\,(T_{ext} - T), \tag{17}$$

where q is the heat flux, h the heat transfer coefficient of air (equal to 5 W/K*m^2) and T_{ext} the ambient temperature. We also apply the *Heat Flux* condition to the foils in order to model the heat flux due to the applied potential as:

$$q_{foil} = \frac{1}{2} q_{tot} = \frac{U^2}{8 * A_{eff} * R}, \tag{18}$$

where U is the potential difference applied to both heaters, A_{eff} = 5.1 cm^2 is the effective area of each foil given by the manufacturer and R = 5.6 Ohm is the resistance of each heater. In this way we consider the fact that each heater dissipates half of the total heat given by the presence of the total applied potential. Another boundary condition applied to the heaters is the *Highly Conductive Layer* node that is used to model heat transfer in thin layers. The equation of this node describes the in-plane heat flux in the layer:

$$d_s \rho_s C_s \frac{dT}{dt} + \nabla_t \cdot (-d_s k_s \nabla_t T) = q_{\partial\Omega} - q_\Omega + d_s Q_s = -q_s, \tag{19}$$

where ρ_s is the layer density, C_s the layer heat capacity, k_s the layer thermal conductivity at constant pressure, d_s the layer thickness, $q_{\partial\Omega}$ the heat flux from the surrounding into the layer, q_Ω the heat flux from the layer into the domain, Q_s represents internal heat sources and q_s is the net outflux of heat [18].

In the following the results obtained from simulations of the heating of the baseplate are presented. In Fig. 3.2, the results from stationary studies can be observed, clearly showing that the temperature of the system rises as we increase the potential applied to the heating foils. As suggested by the small color gradients in each image, the temperature profile remains quite homogenous along the whole baseplate for different heater voltages, with the temperature being a little bit higher near the foils. We can also calculate the average surface temperature: this is a particular feature of COMSOL that allows you to obtain the average value of a domain. In this case, if we consider Fig. 3.2 b), and if we apply this tool at different sections of the baseplate, we obtain that there is a difference of 0.5 °C between the value registered at the temperature sensor position and the one near the heating foil, while the difference is only 0.2 °C with respect to the central part of the baseplate (Fig. 3.3).

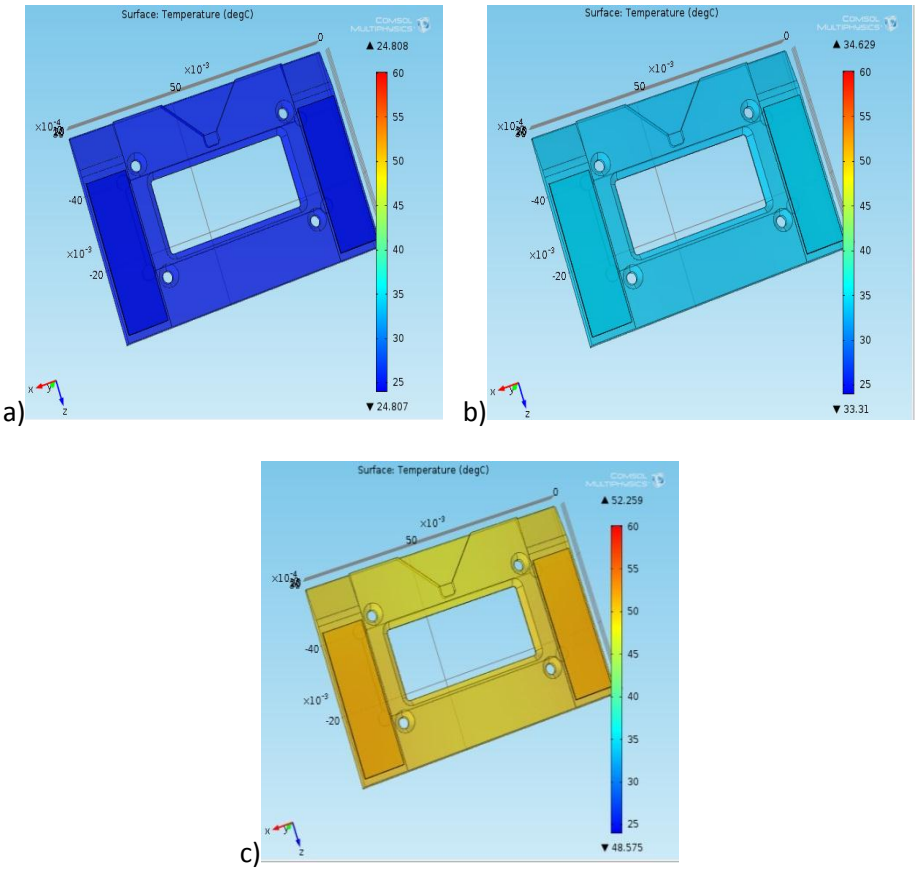

Fig. 3.2: *Results obtained from stationary studies of the heating process (corresponding to an infinitely long equilibration time). a) Voltage applied 0.1 V, temperature at the sensor position 24.81 °C; b) Voltage applied 3 V, temperature at the sensor position 33.34 °C; c) Voltage applied 5 V, temperature at the sensor position 48.65 °C. Color scale range for all images [24; 60] °C.*

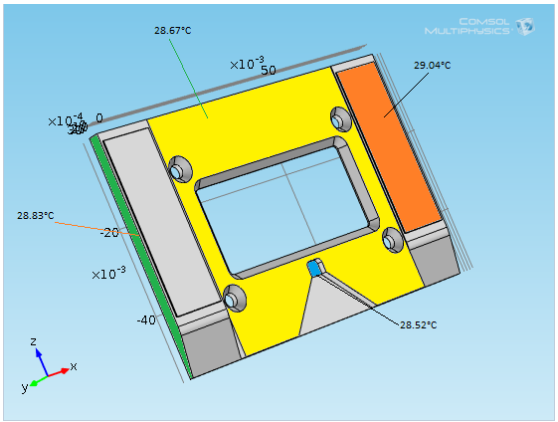

Fig. 3.3: *Average surface temperature at different sections of the baseplate in a stationary study (see Fig. 3.2 b). Voltage applied: 2V.*

Here the results obtained from time-dependent studies of the heating process are presented. In this case the simulations show that the system needs more or less 60 min to reach a stable temperature value at the position where the Pt100 temperature sensor is located.

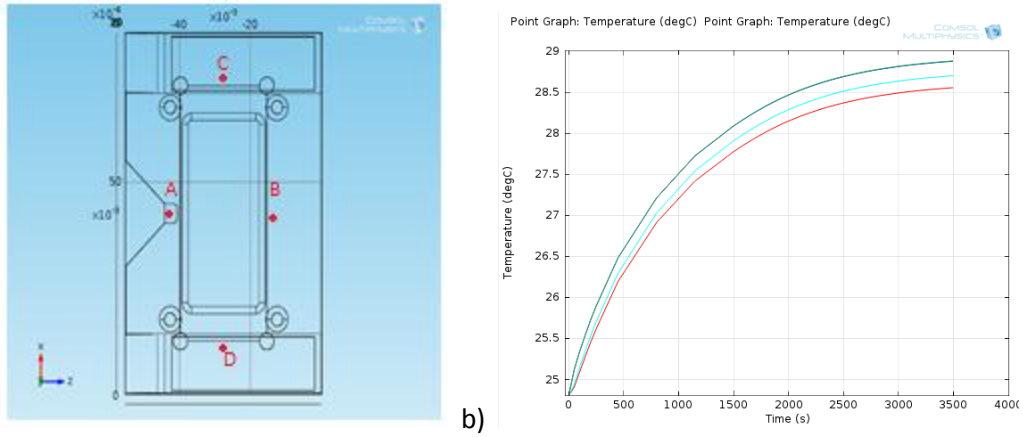

Fig. 3.4: *Results obtained from time-dependent studies of the heating process (Voltage applied: 2 V). a) The red spots indicate the points where the curves of b) are taken. (A = light blue, B = red, C = green, D = blue; C and D are coincident).*

The data obtained from the simulations of the heating are in agreement with the experimental ones that will be presented in the next subsection (see Fig. 3.5). Comparing the results obtained from stationary simulations and experimental temperature values registered when the system is stabilized, we can say that i) the dependence between the temperature and the applied voltage is quadratic for both cases, and ii) the agreement is better for voltage values smaller than 5V, maybe due to the fact that for larger voltages heat dissipation to the environment becomes predominant during experiments and the system cannot follow the ideal behavior predicted by the simulations anymore.

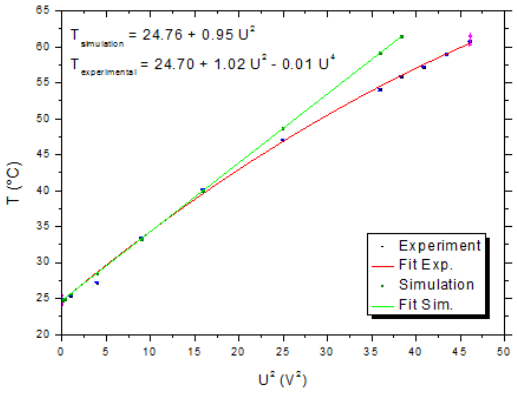

Fig. 3.5: *Comparison between the squared voltage dependences of the temperature obtained from simulations (green) and experiments (red) (see section 3.2).*

However, it is important to underline that the way in which we model the heating foils is not completely correct because we apply the *ec* module to the polyimide layer instead to the resistance placed inside two layers of this insulator material (see section 2.2). So we may need to improve our description and check if it is possible to obtain a better agreement. In any case, the results obtained from the simulations show values that are compatible with the ones obtained from experiment: we can identify a small gradient in

temperature that can be seen experimentally. In summary, these results are a good starting point in order to achieve an optimum description of the real system, which turns out to be complicated.

3.2 Calibration experiments for temperature control

Before using the modified sample cell in MT experiments, some preliminary measurements are needed to i) characterize the voltage-temperature dependence after long equilibration times, ii) to determine the optimum parameters for the PID feedback, iii) to check the response of the system to setpoint changes (with the feedback tuned on), and iv) to probe if the system heats-up homogenously at different points of the baseplate.

Voltage-temperature characteristics

In order to find the relation between the voltage *U* applied to the heating foils and the temperature *T* of the baseplate, we monitor how the temperature changes as the voltage is increased stepwise. We do that by using two small separate LabVIEW programs: one to monitor the temperature readout and one to set the voltage from the power supply. The *U*-*T* relationship obtained is then implemented in the main software program that controls the whole system (see chapter2) and, converts a temperature setpoint into a voltage setpoint. It is also possible to estimate a linear sensitivity *S* [°C/V] of the system, which is the coefficient used within the PID feedback to calculate the controller output given in Volts according to Eq. 16.

The procedure of this first calibration measurement is as follows. We increase the voltage starting from 0 V, with steps of 1 V, and we register temperature values after an adequately long time of about 20 min: this time is enough for the system to stabilize. We increase the voltage up to a value of about 6.8 V, which corresponds to a temperature of 60 °C in the central region of the baseplate. Since we cannot cool down the system actively, we also monitor the temperature for decreasing voltages, which behaves slightly differently. Here the curves that relate the temperature to the voltage and the corresponding fitting formulas to be used in the main software program are presented. Note that in Fig. 3.5 the temperature is plotted as a function of the squared voltage, which is proportional to the heating power and should give rise to a linear relationship. In order to account for increased heat dissipation at high voltages, we prefer however to fit the data with a polynomial.

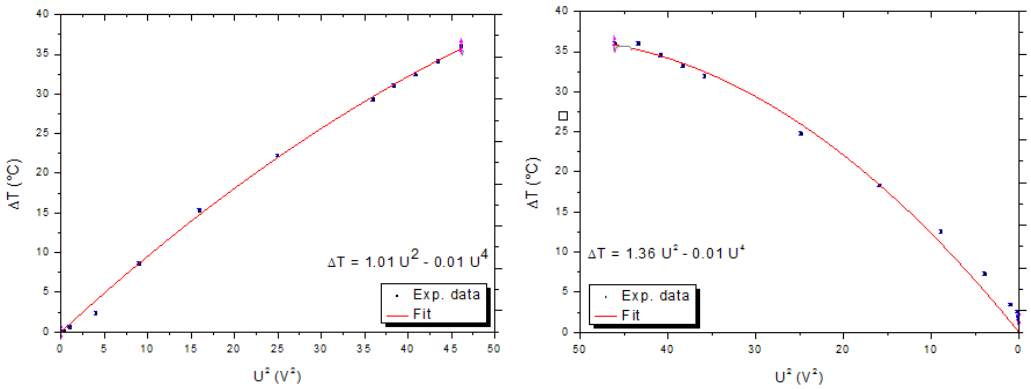

Fig.3.6: *Plot of the experimental data of the temperature difference between the registered value and the ambient one as a function of the squared voltage for increasing voltages (left) and for decreasing voltages (right).*

The inverse relations that we obtain from the fits are:

$$U = 0.5\sqrt{403.1 - 2.0\sqrt{40616.8 - 803.2T}}\text{, for increasing voltages} \quad (19)$$

$$U = 0.5\sqrt{215.9 - 2.0\sqrt{11651.0 - 317.5T}}\text{, for decreasing voltages} \quad (20)$$

These two equations are rather similar when plotted (data not shown). For this reason, we decide to use the first one to calculate the initial voltage setpoints in the LabVIEW program. Use of the second formula did not change our results. Also, we obtain an approximate sensitivity for both cases:

$$S = \frac{T_{max} - T_0}{V_{max} - V_0}, \quad (21)$$

where T_{max} is the maximum temperature reached at the maximum applied voltage V_{max} and T_0 is the value at $V_0 = 0$ V. We estimate $S = 5.3\ ^{\circ C}/_{V}$ for increasing voltages and $S = 5.1\ ^{\circ C}/_{V}$ for decreasing voltages and use both values for our PID feedback.

Determination of optimum PID parameters

We use both techniques mentioned in chapter 2 to obtain the best combination of values to control the response of the system. The steps followed are described below [19]:

CLOSED-LOOP TECHNIQUE:

1. With the temperature having settled at a certain value, the control program has to be switched to PID mode, with *I* and *D* set to zero.
2. Without changing the temperature setpoint, the *P* gain has to be set to a small value.
3. Monitoring the temperature, *P* has to be slowly increased until the process starts to oscillate.
4. The value of *P* at which oscillations are first observed is called the ultimate gain K_u and its corresponding oscillation period T_u has to be monitored.

5. Using the following relations it is possible to obtain *P*, *I* and *D* from K_u and T_u:

$$P = \frac{3K_u}{5}; I = \frac{2}{T_u}; D = \frac{T_u}{8} \tag{22}$$

OPEN-LOOP TECHNIQUE:

1. The control program has to be switched to manual mode (PID off).
2. Before starting the measurement, it is necessary to wait that the process is stable at the initial control signal (i.e. voltage) value.
3. At t = 0 s a small (voltage) step change is made and the measured process signal (i.e. temperature) has to be recorded until it stabilizes.
4. The function *h(t)* (see Fig. 3.6) has to be plotted as a function of time.

$$h(t) = \frac{Measure\ (t) - Measure(t=0)}{Measure(t=t_f) - Measure\ (t=0)} \tag{23}$$

where t_f refers to the stabilization time of the process after the step change.

5. From the plot the values of *a* and *L* are obtained as show in the figure:

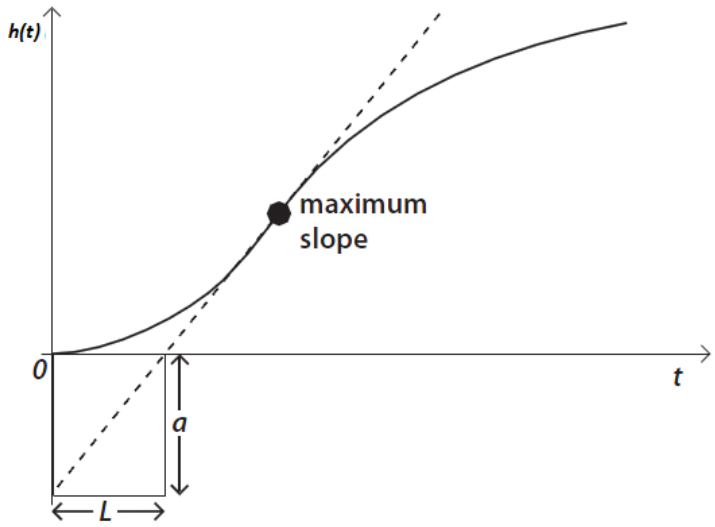

Fig. 3.7: *Concept of graphical data analysis corresponding to the open-loop technique, taken from Ref. [19].*

6. Using the following relation it is possible to obtain *P*, *I* and *D* from *a* and *L*:

$$P = \frac{1.2}{a}; I = \frac{1}{2L}; D = \frac{L}{2} \tag{24}$$

The best values that we obtain for the PID feedback (see Eq. 16) of our system are: *P* = 0.05; *I* = 0.0001; *D* = 8.0. With these parameters it takes more or less 30 min to stabilize the temperature at the central region of the baseplate after a significant setpoint change.

System response checks

In order to know how the temperature behaves in our PID feedback at different positions of the baseplate, and to check if what we obtained from the simulations is true in reality, we perform measurements of the temperature at different points of the baseplate with the help of a second Pt100 temperature sensor. This second sensor is connected to a second temperature converter, whose signal is read out by the same cDAQ module as described in chapter 2. In this case, however, the temperature sensor is attached to the baseplate using a thermally conductive double-sided adhesive tape, in order to facilitate its detachment. The points where the temperature has been registered are shown in Fig. 3.8.

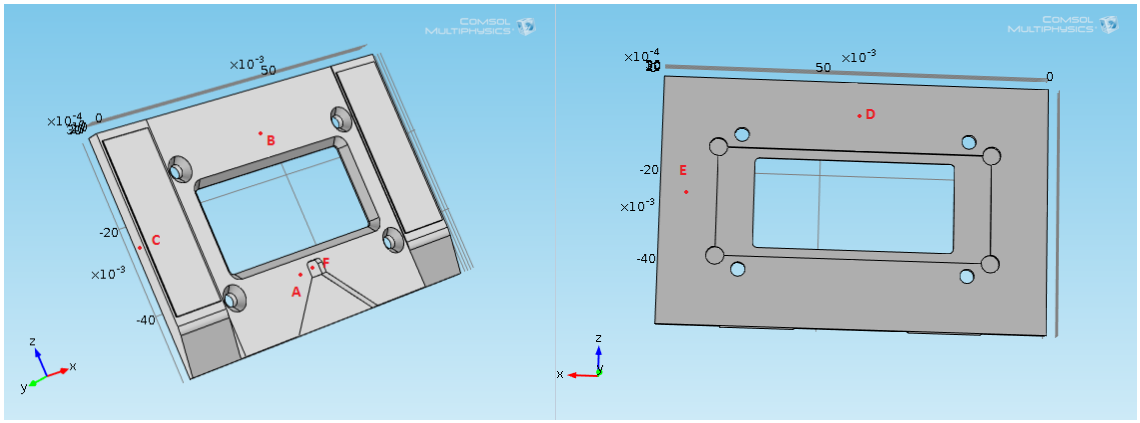

Fig. 3.8: *3D models of the baseplate with heating foils: the red dots show where the second Pt100 sensor has been positioned to probe the temperature gradient.*

To check the calibration of the second sensor, we have monitored the temperature near the position at which the other sensor is glued (position A). In this position the values are smaller than the ones registered at the sensor in position F (with an average difference of 0.13 °C), due to the fact that the fixed sensor (position F) is buried inside the epoxy glue. All the data presented here are corrected by this offset. We obtain that in position C and E the temperature is higher than at the other parts of the system (~0.5 °C), due to the vicinity to the heating foils. In addition, as we produce a step change, the temperature starts to increase faster at points C and E than at point F, as expected. An example of these results is shown in Fig. 3.9a. This behavior corresponds with the one you may expect: the system starts to heat up from the heating foils towards the center, forming a temperature gradient whose amplitude decreases with time. At the other points studied (positions B and D) the temperature difference with the respect to the value at point F is smaller (Fig. 3.9b): more or less 0.2 °C. In summary, the temperature gradient is more pronounced when comparing positions near and far from the heating foils, giving rise to heating responses that are initially “out of phase”. Using the temperature signal from the Pt100 sensor fixed at an equal distance to both the heating foils, with our previously determined PID parameters the system needs about half an hour to stabilize.

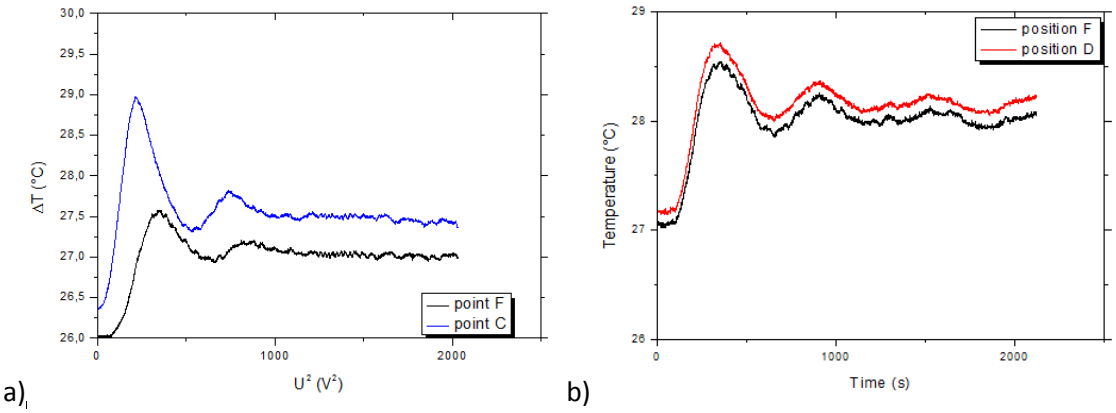

Fig. 3.9: *Temperature responses with PID feedback comparing a) the signals from the fixed Pt100 sensor and at position C (step change 1°C from 26 °C to 27 °C) and b) the signals from the fixed Pt100 sensor and at position D (step change 1°C from 27 °C to 28 °C). Sample rate 2Hz.*

4. Conclusions and Outlook

The results presented in this M.Sc. thesis correspond to the initial steps towards a temperature-controlled sample cell assembly for single-molecule experiments. Before being able to use it in our MT setup other tests need to be done. One of them being the measurement of the temperature inside the fluid cell filled with buffer. In a previous step however, and as suggested in the article by Baker et al. [20], what we can do to estimate the temperature inside the cell without buffer is to introduce a wax with a well-defined melting temperature and observe its change in appearance as it changes from the solid to the liquid state. In preliminary experiments, we have mounted a sample cell containing wax together with the complete holder part assembly (see Fig. 2.2) on the MT and monitored the temperature of the system while heating the baseplate. Our goal was to quantify the loss of heat in the interior of the cell and at the center of the chamber. From these measurements we have realized that there is a large temperature gradient between the baseplate and the glass cover slides that form the fluid cell, and this is due to strong heat dissipation via the immersion oil drop used for the microscope objective of the MT. We have therefore observed that the complete system (including the fluid cell) behaves differently in comparison to the baseplate alone (see chapter 3). On the other hand, in a real experiment and in contrast to the measurement with the wax, the sample cell will be filled with buffer. Presumably, the dissipation will be different in presence of water and that makes the need to control the temperature inside the channel essential. To achieve this, we are planning to introduce a temperature sensor inside the channel, such that it will be directly in contact with the water solution. Another interesting point will be to understand how all the components of the MT will influence the warm-up process and how much heat the system will dissipate. Apart from that, adding of all the remaining components of the sample cell assembly (such as the PEEK holders and the fluid cell itself) in the simulations will yield valuable complementary information. We can take advantage of the fact that we can model the presence of water in both a steady state and as a flow using the *Microfluidic Module* within COMSOL, in which a laminar flow can be described. To control well all the parameters that influence the temperature of the sample cell system is not easy, but desirable in order to improve the level of understanding of the biological systems that are subject of investigation.

Bibliography:

[1] Keir C. Neuman and Attila Nagy 'Single molecule force spectroscopy: optical tweezers, magnetic tweezers and atomic force microscopy', Nature Methods, Vol.5 No.6, June 2008

[2] C. Carrasco Pulido and F. Moreno-Herrero 'Magnetic Tweezers', ENCYCLOPEDIA OF LIFE SCIENCES 2011

[3] Strick, T. R., Allemand, J. F., Bensimon, D., Bensimon, A., and Croquette, V. (1996). 'The elasticity of a single supercoiled DNA molecule'. Science *271*, 1835-1837.

[4] C. Gosse and V. Croquette 'Magnetic Tweezers: Micromanipulation and Force Measurements at the Molecular Level', Biophysical Journal, Vol.82, June 202, 3314-3329

[5] S.S. Patel and I. Donmez 'Mechanisms of Helicases' Journal of Biological Chemistry Vol.281, No.27, pp.18265-18268, July7, 2006

[6] Joseph T.P. Yeeles et al. 'Recombination Hotspots and Single-Stranded DNA Binding Proteins Couple DNA Translocation to DNA Unwinding by the AddAB Helicase-Nuclease' Molecular Cell 42, 806-016, June 24, 2011

[7] www.nature.com

[8] J.T.P.Yeeles and M.S.Dillingham, 'A Dual-nuclease Mechanism for DNA Break Processing by AddAB-type Helicase-nucleases, J.Mol.Biol 271, 66-78(2007)

[9] Joseph T.P. Yeeles et al. 'The AddAB helicase-nuclease catalyses rapid and processive DNA unwinding using a single Superfamily 1A motor domain' Nucleic Acids Research, 2011, Vol. 39, No.6 2271-2285

[10] R. Seidel et al. 'Motor step size and ATP coupling efficiency of the dsDNA translocase EcoR124I' The EMBO Journal (2008) 27, 1388-1398)

[11]Minco 'Flexible heaters design guide'

[12] James P. Hartnett 'Advances in Heat Transfer, Volume 36'

[13] www.correge.fr

[14] www.uniteksys.com

[15] www.iqinstruments.com

[16] www.ni.com

[17] D. Sellers 'An Overview of Proportional plus Integral Plus Derivative Control and Suggestions for Its Successful Application and Implementation'

[18] www.comsol.com

[19] Stanford Research Systems, ‘Analog PID controller SIM 960’ User manual review, revision 2.0, 2006

[20] Matthew A. B. Baker, Yuichi Inoue, Kuniaki Takeda, Akihiko Ishijima, Richard M. Beyy, ‘Two methods of temperature control for single-molecule measurements’ European Biophysics Societies Association 2011